Available online at www.sciencedirect.com
SCIENCE DIRECT®
Journal of Catalysis 233 (2005) 123–135
JOURNAL OF CATALYSIS
www.elsevier.com/locate/jcat

Selective oxidation of benzene to phenol with nitrous oxide over MFI zeolites. 1. On the role of iron and aluminum

E.J.M. Hensen [a,*], Q. Zhu [a], R.A.J. Janssen [b], P.C.M.M. Magusin [a], P.J. Kooyman [c], R.A. van Santen [a]

[a] *Schuit Institute of Catalysis, Eindhoven University of Technology, P.O. Box 513, 5600 MB, Eindhoven, The Netherlands*
[b] *Laboratory of Macromolecular and Organic Chemistry, Eindhoven University of Technology, P.O. Box 513, 5600 MB, Eindhoven, The Netherlands*
[c] *National Centre for High Resolution Electron Microscopy, Delft University of Technology, Julianalaan 136, 2628 BL, Delft, The Netherlands*

Received 12 October 2004; revised 30 March 2005; accepted 8 April 2005

Available online 23 May 2005

Abstract

Three MFI zeolites with iron ([Fe]MFI), aluminum ([Al]MFI), or a combination thereof ([Fe,Al]MFI) as framework substituents were hydrothermally synthesized. The evolution of the iron and aluminum species during template removal and further hydrothermal activation was carefully studied by UV–vis, ESR, ^{27}Al NMR, infrared spectroscopy, and high-resolution TEM. Directly after synthesis, Fe and Al appear to be incorporated to a large extent into the zeolite framework. Iron is clearly less stable at framework positions than aluminum. The migration of iron to extraframework positions readily proceeds during template removal. Although a large fraction of framework iron is removed upon calcination in [Fe]MFI and [Fe,Al]MFI, the extent of Fe^{3+} clustering is more pronounced in the latter material. A more severe steam activation step is required to extract a substantial amount of aluminum from framework positions. In contrast to [Al]MFI and [Fe]MFI, [Fe,Al]MFI shows good performance in selective oxidation of benzene to phenol. A comparison of IR spectra of adsorbed NO_2 groups points to the presence of various extraframework species. After the activation of [Fe,Al]MFI an extraframework mixed metal oxide species is formed, which is argued to be essential for selective oxidation of benzene to phenol with nitrous oxide.

Keywords: Zeolite; MFI; Iron; Aluminum; Selective oxidation; Benzene; Phenol; Nitrous oxide; Active sites; UV–vis; ESR; Al NMR

1. Introduction

Zeolites are porous aluminosilicates made of corner- and edge-sharing SiO_4 and AlO_4 tetrahedra. Charge compensation of the negatively charged aluminum-containing tetrahedra by protons results in strong Brønsted acidity, which is widely applied to upgrade hydrocarbon feedstocks [1,2]. Transition-metal ions dispersed in the zeolite micropore space endow these materials with a wider application window. Interesting examples include dehydrocyclization of alkanes with Ga or Zn [3,4], ammoxidation of ethane with Co [5,6], and reduction of NO_x by hydrocarbons [7–11] or ammonia [12,13] with Co or Fe.

In the last decade, selective oxidation of aromatics by nitrous oxide over iron-containing MFI materials has attracted considerable attention [11,14–18]. A related application is the low-temperature decomposition of nitrous oxide [19], which may find application in the cleanup of tail gases of nitric acid plants. There has been a wide range of studies of the preparation, activation, and catalytic activity of such materials [7–11,14–41]. However, the nature of the active species remains a moot point. The most important proposals for the active species are extraframework Fe species [14,15], Brønsted acid sites [24], and Lewis acid Al sites [21,27]. Recently, attention seems to have gravitated toward the first

* Corresponding author. Fax: +31 40 2455054.
E-mail address: e.j.m.hensen@tue.nl (E.J.M. Hensen).

0021-9517/$ – see front matter
doi:10.1016/j.jcat.2005.04.009

proposal [11,15,16,18,26,28,32,33,36,37,40]. The activity is usually interpreted in terms of very small, possibly dinuclear Fe species stabilized by the negative framework charge of the zeolite [32]. The importance of ferrous ions has been stressed [32,41]. On the other hand, others have found correlations between the amount of extraframework Al species and the catalytic performance [27,29]. Notté [29] noted an optimum balance between the Brønsted acidity and the presence of extraframework iron species for the selective oxidation of benzene to phenol. Others [16] again have suggested that not only Brønsted but also Lewis acid Al sites do not take part in the selective oxidation reaction. Recently we suggested that the active centers consist of ferrous ions stabilized by extraframework Al species [11,18,40,41].

The most important questions pertaining to the active sites for benzene oxidation to phenol regard (i) the importance of iron and (ii) the role of aluminum, if any, and its location (framework or extraframework). Several studies on HZSM-5 zeolites [21,24,27] have used commercial zeolite starting materials that often contain nonnegligible amounts of iron. In other cases, the reported levels of Fe also cannot be neglected. Conversely, it has proved difficult to prepare aluminum-free Fe-silicalite [17,23]. Thus, it appeared important to synthesize and compare pure aluminosilicate, ferrisilicate, and ferrialuminosilicate zeolites. We reported the catalytic performance of such zeolites in an earlier contribution [18] and have shown that self-reduction of iron only takes place for the ferrialuminosilicalite material by X-ray absorption near-edge spectroscopy [41]. In this study we present more details of the preparation, activation, and catalytic activity of these materials. UV–vis, ^{27}Al NMR, ESR, infrared spectroscopy, and TEM were used to characterize the various zeolites. Finally, catalytic reactions involving the activation of nitrous oxide, that is, nitrous oxide decomposition and selective oxidation of benzene to phenol, were performed to relate the structural characterization to the catalytic performance.

2. Experimental

2.1. Catalyst preparation

All synthesized zeolites are denoted by the abbreviation MFI, which refers to their framework topology. [Fe]MFI (iron-substituted silicalite), [Al]MFI (HZSM-5), and [Fe, Al]MFI (iron-substituted ZSM-5) were prepared by controlled hydrolysis of tetraethylorthosilicate (TEOS) in the presence of tetrapropylammonium hydroxide (TPAOH). To this end, 102.4 g TEOS (Acros, 98%) was added to 150 g TPAOH (Fluka, 20 wt% in water) and mixed well overnight. An appropriate amount of this solution was subsequently added dropwise to a solution of iron nitrate ($Fe(NO_3)_3 \cdot 9H_2O$, 98%, Merck) and/or aluminium nitrate ($Al(NO_3)_3 \cdot 9H_2O$, 99%, Janssen) with vigorous stirring. The mixture was transferred to a PEEK-lined autoclave and kept at 443 K for 5 days. After filtration, washing, and drying at 383 K overnight, the organic template was carefully removed by the following calcination procedure: (i) an amount of zeolite was treated in 100 ml min^{-1} N_2 during heating to 823 K at a ramp rate of 1 K min^{-1} and kept at this temperature for 8 h; (ii) the material was further treated in 100 ml min^{-1} 20 vol% O_2 in N_2 at 823 K for another 4 h. To study the evolution of Fe and Al species during template removal, several zeolite samples were taken out for further characterization at different stages of the calcination process. Steam activation of the catalytic materials was achieved by steaming of 1 g of the calcined precursor in a flow of 100 ml min^{-1} 20 vol% O_2 in He with 10 vol% water vapor at 973 K for 3 h. The samples modified by steaming are designated by the suffix (st).

2.2. Characterization

The elemental composition of all samples was determined by ICP analysis. For accurate analysis a known amount of zeolite was fused with lithium tetraborate in Pt crucibles at 1273 K. The fusion tablet was subsequently dissolved in nitric acid. The remnants of the tablet were carefully dissolved in additional nitric acid by gentle heating. The aluminum, silicon, and iron contents of the materials were determined by inductive coupled plasma optical emission spectroscopy (ICP-OES) on a Spectro Ciros^{CCD} spectrophotometer. Powder X-ray diffractograms were measured with a Rigaku diffractometer. Typically, an XRD spectrum was recorded in the range $5° < 2\theta < 50°$ with a scanning speed of 0.01° min^{-1} and Cu-K radiation. Nitrogen adsorption was carried out at 77 K in a Micromeritics ASAP 2000 apparatus. Before nitrogen adsorption, samples were evacuated at 623 K for 16 h.

UV–vis spectra were recorded on a Shimadzu UV-2401 PC spectrometer in diffuse-reflectance mode with a 60-mm integrating sphere. $BaSO_4$ was used as a reference sample. The spectra were transformed into the Kubelka–Munk function, $F(R)$, and subsequently deconvoluted into subbands by standard peak-fitting software. ESR experiments were carried out with a Bruker ESP 300E spectrometer, operating with an X-band standard cavity (9.44 GHz), an ER 035 M NMR Gauss meter, and a HP 5350B frequency counter. A 100-kHz modulation of 5 Gauss and microwave power of 2 mW were used to record the spectra. The field axis was corrected for the variations in frequency in different spectra. The spectra were recorded at 10 K with an Oxford continuous-flow cryostat and variable temperature unit. The spectra were corrected for the sample weight. Magic-angle spinning (MAS) ^{27}Al NMR spectra were obtained on a Bruker DMX-500 spectrometer equipped with a 4-mm MAS probe head, at a magnetic field of 11.7 T. The Al resonance frequency at this field was 130 MHz. The sample rotation speed was 12.5 kHz. The ^{27}Al chemical shifts were referenced to a saturated $Al(NO_3)_3$ solution. To obtain NMR spectra as quantitatively as possible in the presence of a heterogeneous distribution of quadrupolar coupling constants,

the ^{27}Al nuclei were excited with a single 20° pulse of 1 μs. Excitation pulses longer than 3 μs were seen to overemphasize the extraframework Al signal intensity relative to the framework Al signal. The relaxation delay between scans was set at 1 s. No saturation effects were observed in the spectrum for relaxation delays longer than 0.5 s.

Transmission electron microscopy was performed with a Philips CM30UT electron microscope with a field emission gun as the source of electrons, operated at 300 kV. We mounted samples on Quantifoil carbon polymer supported on a copper grid by placing a few droplets of a suspension of ground sample in ethanol on the grid, followed by drying at ambient conditions.

Infrared spectra of self-supporting 12-mg catalyst wafers were recorded at room temperature on a Bruker IFS-113v Fourier Transform IR spectrometer with a DTGS detector at a resolution of 2 cm^{-1}. Typically, a sample was pretreated in situ in oxygen at a temperature of 823 K for 1 h and cooled to room temperature in vacuo (pressure lower than 10^{-6} mbar), followed by room-temperature exposure to NO (purity > 99.9%, 5 mbar) for 30 min. Finally, the sample was evacuated for 30 min and spectra were recorded at room temperature.

2.3. Activity measurements

Reaction data were collected with a plug flow reactor operating at atmospheric pressure, which is extensively described elsewhere [11]. For nitrous oxide decomposition, 0.08 g of catalyst (sieve fraction 125–425 μm) was diluted with SiC to meet plug flow requirements. A well-calibrated online quadrupole mass spectrometer (Balzers TPG-215) was applied for analysis of the gas-phase components. Typically, 0.5 vol% N_2O in He (Hoekloos) was used as the feed gas. The hourly space velocity of the gas was 30,000 h^{-1}. Before reaction, the catalysts were calcined in artificial air (20 vol% O_2 in He, 100 ml min^{-1}) during heating from room temperature to 823 K. After an isothermal period the catalyst was cooled to the reaction temperature. For nitrous oxide decomposition, the starting reaction temperature was 473 K. The heating rate during temperature-programmed nitrous oxide decomposition was 5 K min^{-1}.

For the oxidation of benzene to phenol by nitrous oxide, typically 0.1 g of catalyst (sieve fraction 125–425 μm) was mixed with SiC. Benzene was fed to the reaction mixture by a liquid mass flow controller (Bronkhorst). The final feed mixture contained 1 vol% benzene and 4 vol% nitrous oxide in helium and was fed at a total flow rate of 100 ml min^{-1}. The hourly space velocity of the gas was 30,000 h^{-1}. All valves and most tubing of the reaction system were placed in an oven system and heated to 453 K to avoid condensation of heavy product molecules. The gas-phase composition was determined by a combination of online gas chromatography (Hewlett-Packard GC-5890 equipped with an HP-5 column, FID) and a mass spectrometer system (Balzers TPG-215). The reaction products included phenol, water, carbon monoxide, and carbon dioxide. We determined the nitrous oxide and benzene conversions, the nitrous oxide selectivity (the fraction of oxygen atoms from nitrous oxide incorporated in phenol), the benzene selectivity (the fraction of benzene converted to phenol), and the rate of phenol formation. The carbon and nitrogen mass balances closed at 98% after prolonged reaction times.

3. Results

3.1. Characterization

All synthesized materials were white powders exhibiting the typical X-ray diffraction pattern of zeolites with the MFI topology. No typical diffraction peaks due to iron oxide aggregates were found. The elemental compositions of the zeolite samples are listed in Table 1. Clearly, the use of tetraethylorthosilicate offered a route to relatively pure aluminosilicalite with an iron content of less than 0.001 wt%. The aluminum content in [Fe]MFI is negligible, in contrast to commonly applied synthesis methods that result in aluminum contents of 0.01–0.04 wt%. The iron and aluminum contents of [Fe,Al]MFI are close to the iron content in [Fe]MFI and the aluminum content in [Al]MFI. Table 1 also reports the analysis results of the nitrogen adsorption isotherms for the calcined zeolites and [Fe,Al]MFI(st). The differences between the various samples were relatively small. Careful inspection of the adsorption isotherms indicated that the somewhat higher external surface areas of [Fe]MFI and [Fe,Al]MFI(st) are not due to the creation of a large portion of mesopores. The surface areas and micropore volumes of these materials and those of a commercial HZSM-5 zeolite that was extensively characterized in previ-

Table 1
Elemental composition, surface area, micropore volume and external surface area of the various hydrothermally synthesized zeolites as determined by ICP-OES and nitrogen adsorption

Catalyst	Al content (wt%)	Fe content (wt%)	Si/Al	Si/Fe	S_{D-R} ($m^2\ g^{-1}$)	V_{D-R} ($cm^3\ g^{-1}$)	S_{ext} ($m^2\ g^{-1}$)
[Al]MFI	0.88	< 0.001	42	–	397	0.141	131
[Fe]MFI	< 0.005	0.55	–	143	409	0.146	157
[Fe,Al]MFI	0.92	0.51	40	147	401	0.143	138
[Fe,Al]MFI(st)	n.d.[a]	n.d.	n.d.	n.d.	413	0.147	145

[a] Not determined.

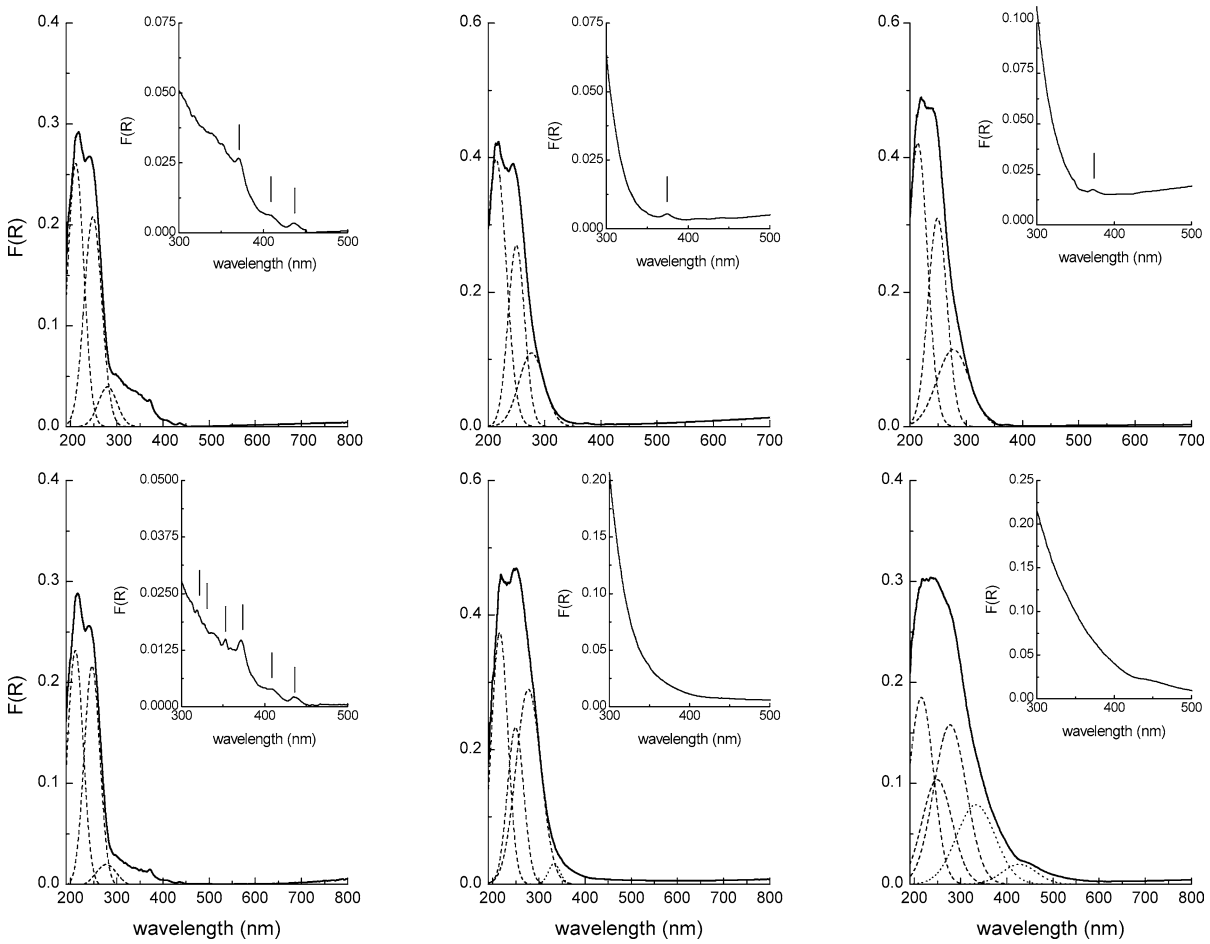

Fig. 1. UV–vis spectra of (top) [Fe]MFI and (bottom) [Fe,Al]MFI for (left) as-prepared, (middle) calcined in artificial air at 823 K and (right) steamed at 973 K. The inset shows a magnification of the region of the *d–d* transitions and indications of the main features.

ous studies [11,40] were close and permit a comparison of the catalytic activities.

The coordination state and extent of aggregation of Fe^{3+} in the iron-containing zeolites were investigated by UV–vis spectroscopy [25,46–48]. Fig. 1 displays the optical spectra of [Fe]MFI and [Fe,Al]MFI. Overall spectra of the as-synthesized materials, the materials obtained after template removal, and those obtained after steaming activation are compared, and a more detailed view of the spectra in the region of the *d–d* transitions is also presented. The spectra of the as-synthesized zeolites are dominated by two characteristic oxygen-to-metal charge-transfer (CT) bands for Fe^{3+} around 211 and 245 nm, which are characteristic for Fe^{3+} at isolated tetrahedral framework sites [25]. For the as-synthesized materials a considerable background at higher wavelengths is observed, which should be due to a variety of *d–d* transitions with slightly different coordinations. After calcination the CT maxima shifted slightly to higher wavelengths, which may be interpreted in terms of an increased number of oxygen ligands [25,45]. This implies that (part of) Fe^{3+} migrated from framework to extraframework positions. At the same time, a shoulder around 280 nm is observed that has been attributed to isolated octahedral Fe^{3+} complexes [25]. To follow these changes in more detail, the UV–vis spectra were deconvoluted into various subbands. Two CT bands were used below 260 nm for isolated Fe^{3+} species and three bands at fixed wavelengths of 277, 333, and 427 nm for isolated octahedral Fe^{3+} complexes, octahedral Fe^{3+} in oligomeric clusters, and larger Fe_2O_3-like aggregates, respectively [25]. The bands above 260 nm reflect a certain distribution of slightly different cluster geometries [45], corresponding to the broadness of these subbands. The corresponding fit results are collected in Table 2. The CT bands of the isolated Fe^{3+} species shifted to higher wavelengths upon calcination and steaming, pointing to increased coordination due to removal from framework positions. Whereas the as-synthesized zeolites possibly contained a small fraction of isolated octahedral Fe^{3+} complexes in [Fe]MFI and [Fe,Al]MFI, calcination brought about a strong increase in the number of such species. Clearly, the changes were more pronounced for [Fe,Al]MFI than for [Fe]MFI, and a small fraction of more clustered Fe^{3+} was found in calcined [Fe,Al]MFI. Steaming resulted in a further redistribution of Fe^{3+} species in [Fe,Al]MFI, and more extensive clustering into clustered Fe^{3+} species and larger iron oxide aggregates is evident

Table 2
Contributions of subbands below 260 and at 277, 333 and 427 nm derived from deconvolution of UV–vis spectra of [Fe]MFI and [Fe,Al]MFI corresponding to Fig. 1. The maxima (in nm) of the CT bands below 260 nm are indicated between brackets

	$I_{\lambda<260\ nm}$	$I_{\lambda=277\ nm}$	$I_{\lambda=333\ nm}$	$I_{\lambda=427\ nm}$
[Fe]MFI as-synthesized	92 (212, 245)	8	–	–
[Fe]MFI calcined	82 (215, 249)	18	–	–
[Fe]MFI steamed	78 (215, 249)	22	–	–
[Fe]MFI steamed, severe[a]	68 (215, 249)	27	5	–
[Fe,Al]MFI as-synthesized	94 (211, 245)	6	–	–
[Fe,Al]MFI calcined	58 (215, 250)	40	2	–
[Fe,Al]MFI steamed	47 (215, 249)	31	18	4

[a] [Fe]MFI activated at 1073 K in 30 vol% water vapor.

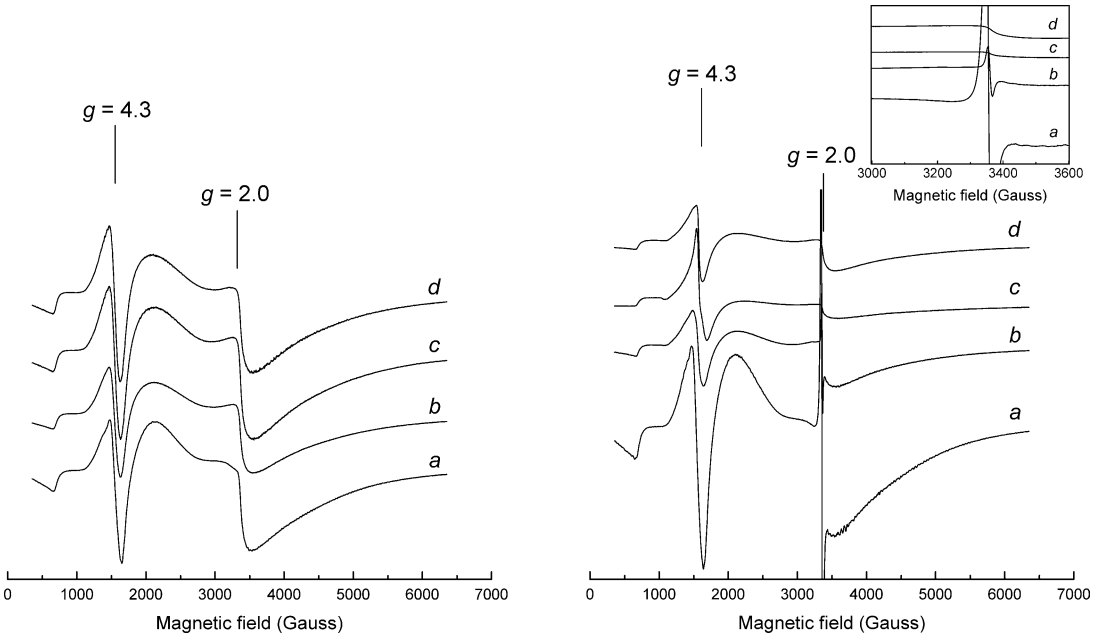

Fig. 2. ESR spectra of (left) [Fe]MFI and (right) [Fe,Al]MFI, (a) as-prepared, (b) treated in N_2 up to 673 K, (c) calcined in artificial air at 823 K and (d) steamed at 973 K. The inset shows a magnification around $g = 2.0$ for [Fe,Al]MFI.

from the higher intensity of the band at 333 nm and the appearance of a subband at 427 nm, respectively. Contrarily, the extent of clustering in [Fe]MFI upon steaming was much less pronounced. We found that in calcined [Fe]MFI a considerably smaller amount of isolated octahedral species was formed than in [Fe,Al]MFI. Steaming resulted only in a small increase. These observations are in good agreement with recent results of Pérez-Ramírez [49]. Similarly, further clustering was induced by a more severe steam treatment of [Fe]MFI (1073 K, 30 vol% water vapor), which led to the appearance of clustered Fe^{3+} species, indicated by the band at 333 nm, as derived from the fit parameters in Table 2.

The *d–d* transitions in Fig. 1 are indicative of the tetrahedral environment of Fe^{3+} in the zeolite framework. The bands are partially masked by the tail of one of the CT bands, but in the as-synthesized zeolites the pattern that follows from the d^5 configuration of Fe^{3+} in tetrahedral symmetry [25] is weakly discerned. However, as pointed out by Bordiga et al., this cannot be taken as proof for the exclusive tetrahedral coordination of Fe^{3+} because the Tanabe and Sugano diagrams for tetrahedral and octahedral complexes are quite similar. In fact, for steamed [Fe,Al]MFI a more complex pattern, seemingly consisting of more than five bands, was measured that may derive from bands due to Fe species in different coordination. In both zeolites, these bands became weaker after calcination and steaming, concomitant with an increase in the bands due to clustered species. They largely disappeared in [Fe,Al]MFI, which agrees with the more pronounced Fe^{3+} clustering. On the other hand, the corresponding bands in [Fe]MFI remained weak, even after steaming.

ESR spectra for [Fe]MFI recorded at 10 K for zeolite samples at different stages of the template removal are shown in Fig. 2. The various spectra are quite similar, with minor differences. They all contain two important features at g values of 2.0 and 4.3. Moreover, some weak features are observed in the low-field region. The ESR signal around $g = 4.3$, initially assigned to lattice Fe^{3+} [42,43], belongs

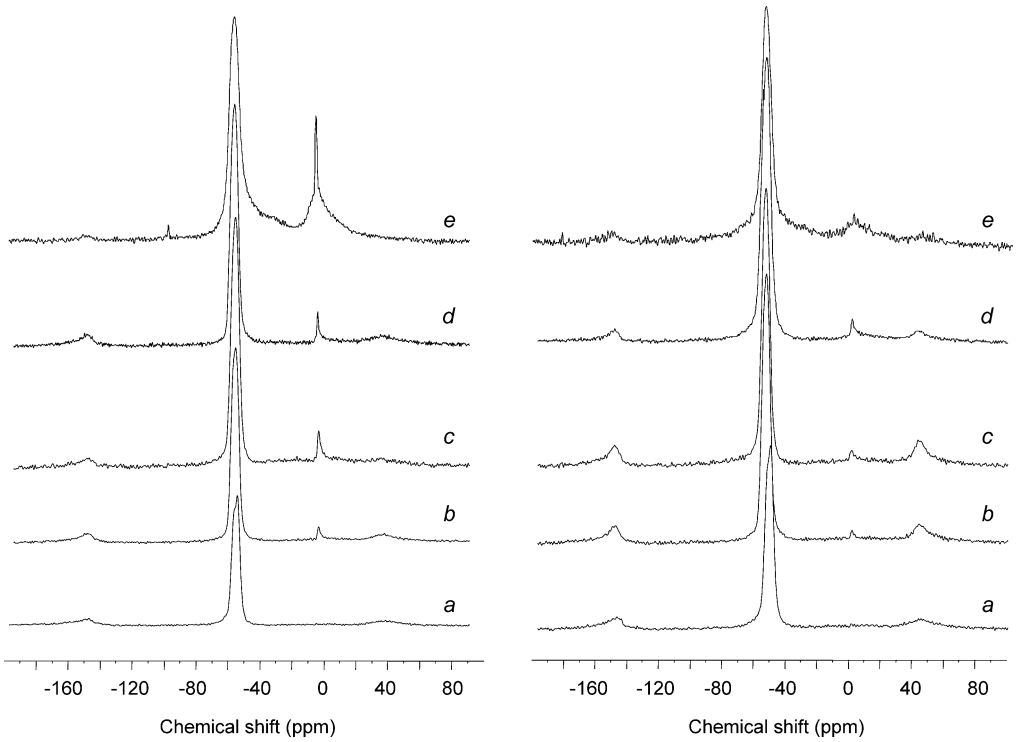

Fig. 3. ^{27}Al NMR spectra of (left) [Al]MFI and (right) [Fe,Al]MFI, (a) as-prepared, (b) calcined in nitrogen at 473 K, (c) calcined in nitrogen at 673 K, (d) calcined in artificial air at 823 K and (e) steamed at 973 K.

to tetrahedrally coordinated ferric ions. This does not necessarily imply that these species are located at framework positions [39,44]. In general, the band at a g value of 2.0 is attributed to Fe^{3+} in iron oxide clusters, where magnetic interactions average out the zero field splitting, although in principle it can also arise from isolated Fe^{3+} ions in high symmetry [45]. The bands in the low field are assigned to higher-coordinated isolated Fe^{3+} ions [45]. Despite the fact that the assignment of the band at $g = 4.3$ is not conclusive, we suggest that the presence of a broad band around a g value of 2.0 directly after synthesis indicates that not all Fe is located in tetrahedral framework positions. After calcination at 823 K of [Fe]MFI, the signal at $g = 2.0$ increased somewhat, which points to further clustering of Fe species in line with a slight decrease in the feature around $g = 4.3$. No severe changes were observed upon steaming [Fe]MFI. The spectrum of as-synthesized [Fe,Al]MFI presents several differences. The more pronounced feature around $g = 2.0$ could point to a higher amount of extraframework Fe species in the precursor as compared with fresh [Fe]MFI. The sharp feature around $g = 2.0$ might indicate a portion of isolated Fe^{3+} ions. The evolution of the ESR spectra upon (hydro)thermal activation is totally different from that of [Fe]MFI. The sharp signal at $g = 2.0$ due to isolated Fe^{3+} species eroded at elevated temperatures. The same applies to the other signals around g values of 2.0 and 4.3. This indicates extensive clustering of iron oxide phases, although in principle partial loss of the Fe^{3+} signal may also explain such behavior. After steam activation we observed an increase in the signal at $g = 2.0$ and a further decrease in the one around $g = 4.3$. This points to more extensive clustering of Fe^{3+}. Here, we cannot discuss in more detail the signals in the low field that were reported earlier [16,36,45] because their resolution is too weak.

Table 3
Quantitative analysis of the ^{27}Al NMR spectra of [Al]MFI and [Fe,Al]MFI corresponding to Fig. 3. All signals are normalized to the resonant signal of as-prepared [Al]MFI

Catalyst	Treatment	Al(IV)[a] (%)	Al(VI)[b] (%)
[Al]MFI	As prepared	100	0
	N_2, 473 K	97	3
	N_2, 673 K	97	3
	O_2/N_2, 823 K	95	5
	Steam, 973 K	65	35
[Fe,Al]MFI	As prepared	90	0
	N_2, 473 K	78	1
	N_2, 673 K	55	1
	O_2/N_2, 823 K	37	1
	Steam, 973 K	33	8

[a] Al(IV) refers to tetrahedrally coordinated aluminum, characterized by a chemical shift around 52 ppm.
[b] Al(VI) refers to octahedrally coordinated aluminum with a chemical shift close to 0 ppm.

NMR spectra of [Al]MFI are presented in Fig. 3, and quantitative data are condensed in Table 3. The bands at 0 ppm and 52 ppm are commonly assigned to octahedral extraframework and tetrahedral framework Al species, respectively. The spectrum of fresh [Al]MFI is dominated by one resonance at 52 ppm, which implies that Al is fully incor-

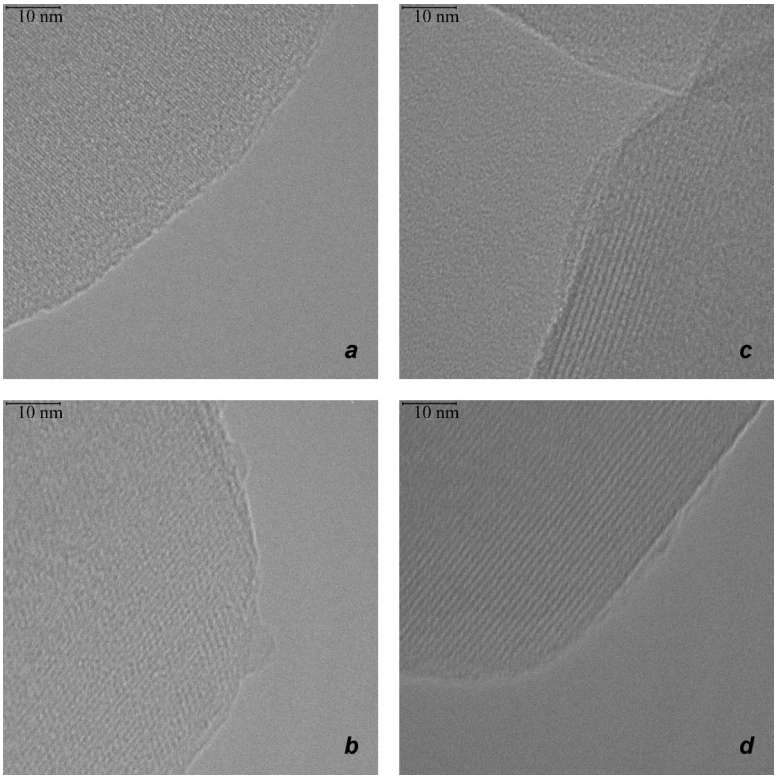

Fig. 4. High-resolution transmission electron micrographs of (a) calcined and (b) steamed [Fe]MFI and (c) calcined and (d) steamed [Fe,Al]MFI.

porated into the framework. The asymmetry of this feature indicates the presence of at least two crystallographically distinct Al sites in the zeolite framework [50]. After treatment in nitrogen at 473 K, a small but distinct peak at 0 ppm appeared. This feature is related to extraframework Al dislodged from the zeolite framework after partial removal of the template. More severe calcination led to an increase in this feature. Approximately 5% of the aluminum atoms were removed from tetrahedral framework positions after complete decomposition of the organic template. Further steaming activation of [Al]MFI brought about more extensive dealumination. Moreover, a new broad peak around 38 ppm appeared, which is usually assigned to a pentahedrally coordinated Al or distorted tetrahedral Al [27]. Fig. 3 also shows the ^{27}Al NMR spectra of [Fe,Al]MFI obtained after various activation treatments. The corresponding quantitative data are given in Table 3. As a result of the paramagnetic nature of the iron species present in [Fe,Al]MFI, part of the Al signal is not visible in the NMR spectrum [34,40]. Nevertheless, similar changes in the ^{27}Al NMR spectra were noted during calcination and steaming of [Fe,Al]MFI. Framework aluminum atoms were progressively removed at elevated temperature, and this dislodgement was more pronounced after steaming. The quantitative data in Table 3 further underline the loss of resonant area. For instance, the total resonant area in [Fe,Al]MFI calcined at 823 K amounted to only one-third of the signal in [Al]MFI. The ratio of octahedral and tetrahedral Al ions in [Fe,Al]MFI is substantially lower than that in [Fe]MFI. This suggests that a relatively larger part of the extraframework Al nuclei in [Fe,Al]MFI became invisible because of the proximity of paramagnetic Fe centers.

To study the possible clustering of iron oxide aggregates on the external surface, the calcined and steamed forms of [Fe]MFI and [Fe,Al]MFI have been studied by TEM and HRTEM. From TEM micrographs with lower magnification (not shown) we derive that the zeolites are made up of crystals with typical dimensions of 0.3–0.5 μm. The relatively low crystallite size derives from the high TPAOH/Si ratio in the synthesis gel; the alkyl chains of the template favor nucleation [51]. Whereas [Fe]MFI consisted of well-formed rounded crystals, these were somewhat more irregular for the aluminum-containing [Fe,Al]MFI materials. In contrast to the calcined zeolites, the creation of mesopores in the steamed zeolites was suggested by the observation of white areas in the HRTEM micrographs [52]. However, the nitrogen adsorption isotherms did not clearly point in that direction. Fig. 4 shows typical high-resolution transmission electron micrographs of the calcined and steamed iron-containing zeolites. In general, iron oxide aggregates on the external surface of the zeolites were not observed. Only in one micrograph (Fig. 4b) for steamed [Fe]MFI were a few agglomerates identified. This result implies that the migration of iron from lattice to extraframework positions was largely limited to the intrazeolite space. This is in line with the interpretation of the UV–vis results showing a small fraction of strongly clustered iron oxides and the visual observation that the samples are white after steam activation. These observations deviate somewhat from those of Pérez-Ramírez

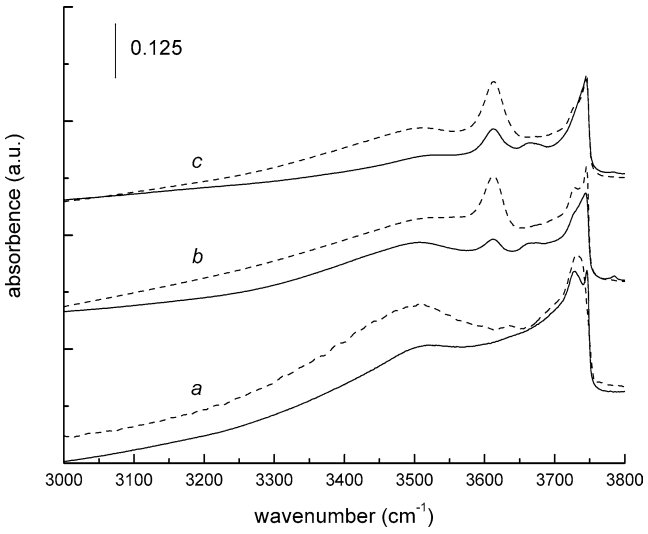

Fig. 5. Infrared spectra of the hydroxyl stretching region of (a) [Fe]MFI, (b) [Al]MFI and (c) [Fe,Al]MFI. Dotted and full lines represent calcined and steamed zeolites, respectively.

et al. [49,53], who clearly observed significant amounts of iron oxide aggregates on the external surface of [Fe,Al]MFI. Pérez-Ramírez also observed such clustered iron oxides for [Fe]MFI after more severe treatment [49].

Fig. 5 shows infrared spectra for the hydroxyl bands of the various calcined and steamed zeolites. The spectra for [Fe]MFI are characterized by bands of isolated silanol groups in the region of 3700–3750 cm^{-1} and a broad signal due to hydrogen-bonded silanol groups with a maximum around 3500 cm^{-1}. In calcined [Fe]MFI we distinguish a weak band at 3630 cm^{-1}, which is related to Brønsted acid hydroxyl groups bridging between silicon and iron framework cations. The higher frequency compared with that of hydroxyl groups associated with framework substitution by aluminum is indicative of its lower acidity. The broad band at lower frequencies is assigned to internal hydroxyl nests deriving from extraction of Fe^{3+} from the framework [25,54]. After steaming, the band at 3630 cm^{-1} can no longer be observed. This indicates further removal of Fe^{3+} from the framework. Moreover, we observe a strong decrease in the broad band around 3500 cm^{-1}, which is due to condensation of internal silanol groups releasing water and forming strained Si–O–Si bridges. Similar effects were also described for Fe-silicalite by Bordiga et al. [25]. The spectra of [Al]MFI present a strong feature at 3610 cm^{-1} due to Brønsted hydroxyl groups bridging between silicon and aluminum. The intensity of the band around 3500 cm^{-1} is much lower, which points to a less defective zeolite structure. This should be attributed to the higher stability of Al in the zeolite framework. A large portion of the Brønsted acid protons disappeared upon steaming, because of the removal of Al from the framework. Together with this decrease, a new signal around 3665 cm^{-1} was observed, which is assigned to hydroxyl groups coordinating to extraframework Al atoms. Again, the intensity in the region

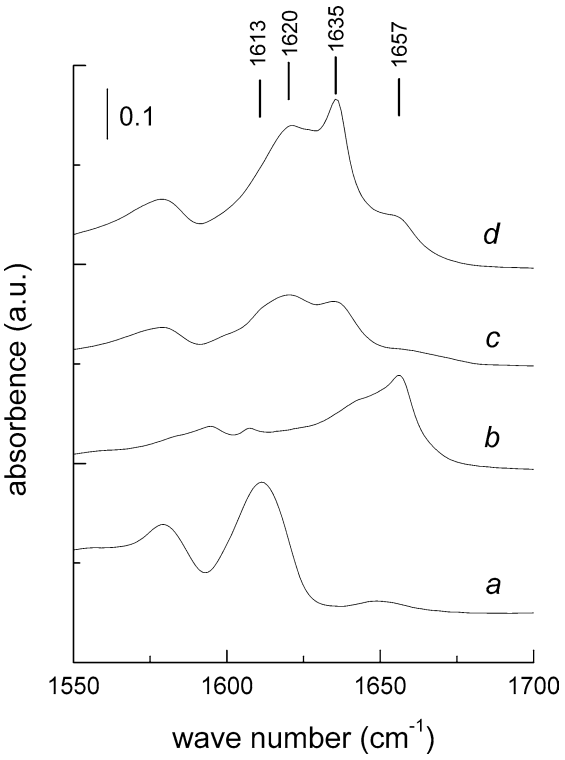

Fig. 6. Room-temperature infrared spectra in the region of 1500–1700 cm^{-1} for (a) [Fe]MFI(st), (b) [Al]MFI(st), (c) [Fe,Al]MFI and (d) [Fe,Al]MFI(st) after exposure to NO for 30 min and subsequent evacuation for 30 min.

below 3600 cm^{-1} decreased. The spectra of [Fe,Al]MFI are dominated by the bands also found in [Al]MFI. Steaming of [Fe,Al]MFI resulted in similar changes due to the removal of framework Al. Nevertheless, the calcined material has a more pronounced feature around 3500 cm^{-1}, which strongly decreased upon steaming, which is similar to the changes in [Fe]MFI. Qualitatively, the extent of dealumination of steamed [Al]MFI and [Fe,Al]MFI appears to be quite similar.

After exposure to NO for 30 min, we observed typical NO bands around 1880 cm^{-1} for all materials. Such bands have been discussed in detail by others [55–62]. In this contribution, we focus on the bands that remain after extensive evacuation after NO exposure. The resulting spectra in the region of 1550–1700 cm^{-1} of the various catalysts are collected in Fig. 6. The bands in this region are due to adsorbed NO_2. Although we initially surmised that these bands derive from a reaction between NO and extraframework oxygen, we alternatively put forward that these bands originate from a NO_2 impurity in the NO feed. The bands below 1600 cm^{-1} are assigned to monodentate/bidentate nitrate groups [56]. The strong band in [Fe]MFI(st) at 1613 cm^{-1} has been assigned to NO_2 interacting with extralattice Fe ions [18]. The pure aluminosilicalite [Al]MFI(st) exhibited a distinctly different IR absorption band around 1657 cm^{-1}. Hence, we suggest that the band is due to NO_2 interacting with extraframework Al species. The weaker feature around 1600 cm^{-1} possibly

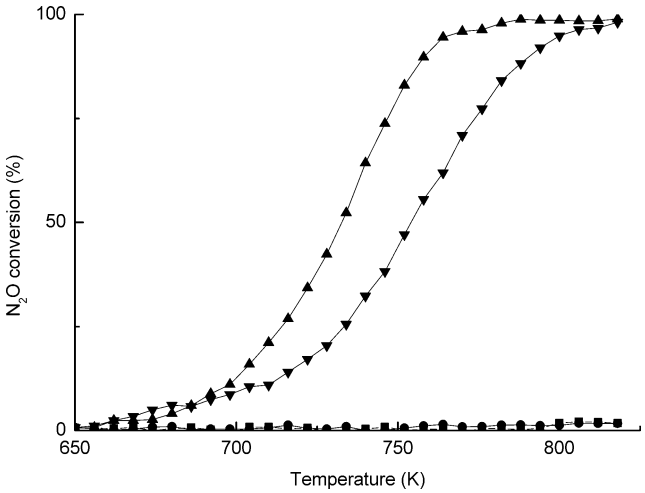

Fig. 7. Temperature-programmed decomposition of nitrous oxide over (■) [Al]MFI(st), (●) [Fe]MFI(st), (▼) [Fe,Al]MFI, and (▲) [Fe,Al]-MFI(st) (feed composition: 0.5 vol% N_2O in balance He at GHSV of 30,000 h^{-1}).

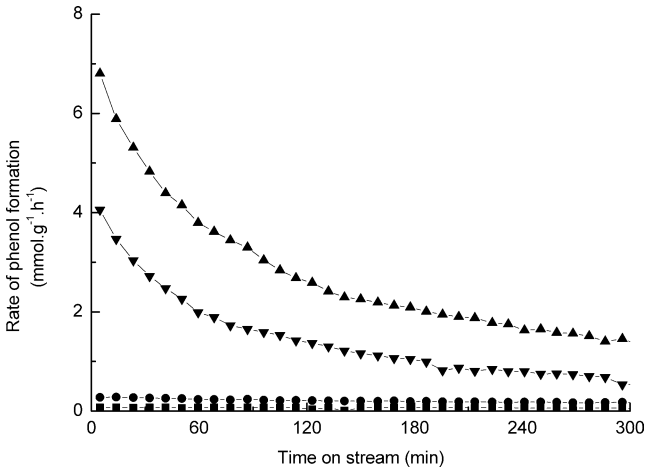

Fig. 8. Rate of phenol formation as a function of reaction time for (■) [Al]MFI(st), (●) [Fe]MFI(st), (▼) [Fe,Al]MFI, (▲) [Fe,Al]MFI(st) (reaction temperature 623 K, feed composition: 1 vol% benzene, 4 vol% N_2O, 95 vol% He, GHSV 30,000 h^{-1}).

relates to nitrate groups [56]. As reported earlier [18], the spectra for [Fe,Al]MFI and [Fe,Al]MFI(st) contain bands around 1612, 1620, 1635, and 1656 cm^{-1}. The first and last band correspond to extraframework Fe and Al species, respectively. The bands around 1620 and 1635 cm^{-1} were assigned to NO_2 interacting with a mixed iron–aluminum-oxide species, as speculated before [55]. This tallies with the observation that such bands only arise for [Fe,Al]MFI and become more pronounced after hydrothermal treatment.

3.2. Catalytic activity

Fig. 7 depicts the conversion as a function of the reaction temperature for [Al]MFI(st), [Fe]MFI(st), [Fe,Al]MFI, and [Fe,Al]MFI(st) during nitrous oxide decomposition. The nitrous oxide conversion of steam-activated alumino- and ferrisilicate remained below 3% at 800 K. The activities of the corresponding calcined materials were similarly low (not shown). [Fe,Al]MFI and [Fe,Al]MFI(st), on the other hand, displayed a significantly higher catalytic activity. The decomposition of nitrous oxide started at approximately 650 K, and full nitrous oxide conversion was reached at 775 K. Steam-activated [Fe,Al]MFI had the highest activity. We stress that [Fe,Al]MFI(st) exhibited a lower activity than a steamed Fe/ZSM-5 catalyst prepared by the sublimation method [11,40].

The rates of phenol formation for the various catalysts as a function of the reaction time at a temperature of 623 K are shown in Fig. 8. Whereas [Al]MFI(st) had a negligible activity and the rate of phenol formation for [Fe]MFI(st) was also very low, [Fe,Al]MFI and [Fe,Al]MFI(st) exhibited a high initial activity; the steamed material had the highest conversion. Deactivation was pronounced, and relatively stable activities were obtained after a reaction time of 3 h. Further reaction parameters (benzene and nitrous oxide conversions and selectivities) are condensed in Table 4. The initial selectivity (after 5 min) of benzene to phenol over [Fe,Al]MFI was approximately 70%, indicating that part of the reactant benzene is converted into products different from phenol. These products were mostly high-molecular-weight coking products, leading to deactivation [37], but also included small amounts of carbon dioxide and water in the initial stages of the reaction. Although the conversion of benzene decreased to 7% after 1 h, the selectivity remarkably increased to values close to 100%.

We attribute the increase in selectivity with decreasing conversion to a consecutive reaction mechanism where ben-

Table 4
Conversion (X) and selectivity (S) for benzene oxidation with itrous oxide for reaction times (t_R) of 5 min, 1, 3 and 5 h (reaction temperature 623 K, gas phase composition 1 vol% C_6H_6, 4 vol% N_2O, 95 vol% He, GHSV 30,000 h^{-1})

Catalyst	C_6H_6		N_2O		C_6H_6		N_2O	
	X (%)	S (%)	X (%)	S (%)	X (%)	S (%)	X (%)	S (%)
	$t_R = 5$ min				$t_R = 1$ h			
[Fe,Al]MFI	22	69	10	36	7	> 98	3	59
[Fe,Al]MFI(st)	38	68	16	42	14	> 98	5	71
	$t_R = 3$ min				$t_R = 5$ h			
[Fe,Al]MFI	4	> 98	3	78	2	> 98	4	83
[Fe,Al]MFI(st)	7	> 98	3	88	6	> 98	3	93

zene is first converted to phenol, followed by its oxidation to dihydroxybenzenes and/or condensation to heavier products. As deactivation due to coke formation is argued to be dominant, the decrease in the amount of available active sites leads to a decrease in the benzene conversion and concomitantly an increase in the selectivity for the intermediate phenol product. [Fe,Al]MFI(st) displayed a reactivity pattern similar to that of [Fe,Al]MFI, but with a higher conversion of benzene (Fig. 8). A comparison with earlier data for sublimed Fe/ZSM-5 materials [11] shows that the present set of materials is more selective and shows a lower deactivation rate than catalysts prepared by sublimation.

4. Discussion

4.1. Structural characterization

[Fe]MFI, [Al]MFI, and [Fe,Al]MFI were successfully synthesized via hydrothermal synthesis. The evolution of the iron and aluminum hetero-atoms during activation was followed by ESR and UV–vis spectroscopy (Fe) and NMR (Al) and infrared spectroscopy (Fe and Al). Iron appears to be less stable as a framework species than aluminum, in agreement with the literature [39]. The lower stability of Fe agrees with its larger ionic radius (0.064 nm for Fe^{3+} vs. 0.050 nm for Al^{3+}). Nevertheless, the agglomeration of Fe species into larger structures was limited, as follows from the predominance of isolated and oligomeric Fe^{3+} species (UV–vis) and the absence of iron oxide particles on the external surface (HRTEM). Moreover, the extent of Fe^{3+} clustering was much smaller in [Fe]MFI than in [Fe,Al]MFI, in line with recent findings of Pérez-Ramírez et al. [49,53]. Infrared spectra of the hydroxyl region, however, confirm UV–vis data that indicate that most Fe^{3+} species have been removed from framework positions after calcination. After steaming, bridging hydroxyl groups associated with framework iron cations were no longer observed.

Directly after synthesis, all Al atoms were incorporated into the framework of the MFI structure in [Al]MFI. A small portion of the tetrahedral Al atoms was lost upon calcination. This dealumination was much more pronounced after steaming, and about one-third of the Al atoms were removed from framework sites. The simultaneous introduction of iron and aluminum into the zeolite framework resulted in a larger destabilization of the zeolite framework. UV–vis spectra suggest that already in the as-synthesized material the amount of Fe at framework locations had noticeably decreased compared with [Fe]MFI. After calcination and complete removal of the template, almost all Fe atoms have migrated to extraframework positions. The evolution of Al atoms in [Fe,Al]MFI zeolites is more difficult to follow by ^{27}Al NMR because of the presence of paramagnetic Fe^{3+}. We observe a lower ratio of detectable octahedral and tetrahedral Al species in calcined and steamed [Fe,Al]MFI compared with the corresponding [Al]MFI zeolites. Tentatively, this may imply that a relatively larger fraction of Fe is closer to extraframework Al species than to framework species. Although it is known that the replacement of protons by metal cations as charge-compensating species increases the framework stability, Rees and co-workers [63,64] earlier proposed that thermal activation of tervalent cations in zeolites like faujasite may lead to dealumination. Experimentally, we observe for [Fe,Al]MFI a similar strong decrease in the infrared band related to bridging hydroxyl groups, as for [Al]MFI. This decrease should at least partly be due to migration of Al to extraframework positions, as follows from the band at 3665 cm^{-1}.

4.2. Catalytic activity

The activity measurements point to large differences in nitrous oxide decomposition rates among the various catalysts. Before and after steaming, [Al]MFI exhibited a negligible nitrous oxide conversion up to temperatures of 800 K. This corresponds to recent data of Pérez-Ramírez et al. [65,66], who found that a similar [Al]MFI material only exhibits significant activity in nitrous oxide decomposition above 800 K. This implies that Brønsted acid sites and Lewis acidic extraframework Al species are not able to activate nitrous oxide at moderate temperatures. In contrast to the reports of Pérez-Ramírez et al. [65,66], we found that [Fe]MFI and [Fe]MFI(st) were not active up to temperatures of 800 K. Pérez-Ramírez et al. reported relatively high activities for steam-activated [Fe]MFI. They concluded that a certain extent of clustering of iron oxide is required for a high activity in nitrous oxide decomposition. We found that the agglomeration of Fe in [Fe]MFI is rather limited. To obtain more insight into this discrepancy, we applied a more severe pretreatment to calcined [Fe]MFI (1073 K, 30 vol% water vapor). The UV–vis spectra point to somewhat more Fe^{3+} clustering (Table 2), but the nitrous oxide decomposition rate of this material was hardly improved. Earlier we proposed that such inactive [Fe]MFI(st) can simply be activated by the addition of Al at extraframework positions [18]. On the other hand, we cannot rule out the possibility that the extent of agglomeration is still lower for the present materials and that this parameter is crucial for good performance in nitrous oxide decomposition [67].

The combination of characterization and activity data points to a strong synergy between Fe and Al in the selective oxidation of benzene to phenol. The activity of [Fe,Al]MFI(st) is considerably higher than that of its calcined counterpart. The positive effect of steam treatment on the decomposition of nitrous oxide has been described before [34,65]. Although generally the beneficial effect of a hydrothermal treatment is thought to derive from additional extraction of Fe from framework positions, we found that a large fraction of iron was already extracted in [Fe,Al]MFI during template removal. This suggests that the increase in activity upon steaming is most likely not due to changes in

the distribution between framework and extraframework Fe species. The samples containing one substituent type, that is, [Al]MFI or [Fe]MFI, produced almost negligible amounts of phenol, whereas [Fe,Al]MFI displayed high rates of phenol formation. Similarly, benzene was not converted over [Al]MFI(st), indicating that Al Lewis sites should also not be considered the active sites. We surmise that the somewhat higher activities of ferrisilicates in benzene oxidation found by others [17,20,68] are related to small quantities of Al in the zeolite samples. [Fe,Al]MFI(st) had a higher rate of phenol formation than [Fe,Al]MFI. The similar reaction parameters suggest that the difference is due mainly to the larger amount of active sites in the steamed catalyst.

It appears that next to the dislodgement of framework Fe, migration of Al from the framework is also essential. This supports our earlier supposition that the active species for selective benzene oxidation consists of a mixed iron–aluminum-oxide species. This contrasts the view of cationic Fe species of low nuclearity as the active sites for benzene oxidation [32]. Instead, we consider the possibility of highly dispersed or mononuclear Fe species stabilized by extraframework Al species, denoted as Fe–O–Al [18]. It may be that these extraframework Fe–O–Al species are stabilized at defect sites of the zeolite.

The importance of high-temperature treatments (calcination or steaming) is probably related to the much higher stability of Al at framework positions compared with that of Fe. Its extraction results in a higher amount of mixed oxide species and a higher catalytic activity. This tentative model is in line with various findings in recent literature. Dubkov et al. [32] have shown that active catalysts can also be obtained by impregnation of $FeCl_3$ into HZSM-5 followed by thermal activation. This suggests that active sites can be created upon removal of aluminum from the framework by steaming at moderate or calcining at very high temperature. This also holds for samples prepared by chemical vapor deposition of $FeCl_3$ onto HZSM-5 [11,40]. Kubánek et al. [16] and Meloni et al. [37] also found a correlation between the presence of extraframework Al sites and catalytic activity, but regarded this as a side effect of the necessary thermal treatments to remove Fe from the framework.

Infrared spectra of adsorbed NO_2 provide additional indications for the formation of a new mixed oxide phase in [Fe,Al]MFI zeolites. Spectra for steamed [Al]MFI and [Fe]MFI produced bands due to NO_2 complexes on extraframework Al and Fe sites, respectively. These bands were less pronounced in [Fe,Al]MFI with similar Fe and Al content. Coupled with their decrease was the appearance of strong new bands around 1620 and 1635 cm^{-1}, which are linked to the presence of extraframework Fe–O–Al. This is supported by the observation that these signals increase after steam activation. Recent works [69–71] also stress the importance of extraframework Al species.

The structure of the Fe–O–Al species remains to be determined. Next to Fe species stabilized to partially dislodged Al sites, one should consider the possibility of stabilization of ferrous ions in aluminates highly dispersed in the zeolite micropores. The most important catalytic property of these Fe-containing sites is their reducibility in the presence of molecular oxygen [32]. The resulting Fe^{2+} species can be titrated by nitrous oxide at temperatures around 523 K. The active site densities lie in the order of 10^{17} to 10^{18} g^{-1}, which corresponds to the involvement of about 0.001–0.01 wt% Fe. We surmise that these sites are made up of mixed Fe–O–Al species and are involved in the selective oxidation of benzene to phenol. It seems unlikely that these few sites are responsible for the high nitrous oxide conversion at higher temperatures. Alternatively, it may well be that other (dispersed) iron-containing phases, that is, cationic iron species and/or agglomerated nanometer-sized iron oxides stabilized in the zeolite micropores [65–67], are able to decompose nitrous oxide at elevated temperatures. In this respect, it is worth noting that even large iron oxide agglomerates can decompose nitrous oxide, starting at a temperature of 723 K. Formation of additional Fe^{2+} sites from such phases at more elevated temperatures should be considered. Indeed, we have shown that, depending on the oxygen partial pressure, catalytic sites are generated at elevated temperatures that can decompose nitrous oxide, but slowly deactivate [11]. The observation that such sites are less abundant upon treatment with higher oxygen partial pressures suggests that these sites may be reoxidized by molecular oxygen and are thus different from the sites responsible for selective oxidation.

5. Conclusions

Trivalent Fe and Al ions can be incorporated into the framework of MFI-type zeolite by introduction of the corresponding metal nitrate salt solutions into the synthesis gel. During subsequent calcination or steaming steps, these substituents are partially removed from framework to extraframework positions. The migration is more evident for Fe than for Al, and a steam treatment is more effective in removing hetero-atoms than the initial calcination step. In short, iron is largely removed during template removal, especially in the presence of aluminum. Clustering of Fe^{3+} species is more extensive in the presence of Al. Considerable amounts of Al are removed only under hydrothermal conditions. The ability of these zeolites to decompose nitrous oxide under mild conditions is limited to those materials containing both Fe and Al. Ferrisilicalite and aluminosilicalite are inactive for selective benzene oxidation to phenol with nitrous oxide. Detailed characterization suggests that extraframework mixed iron–aluminum oxide species are involved in the activation of nitrous oxide at low temperatures and the subsequent benzene oxidation to phenol.

Acknowledgments

The authors are grateful to Dr. M. Sychev (National Technical University of Ukraine, Ukraine) for his valuable guidance in the interpretation of the UV–vis spectra and analysis of the nitrogen adsorption isotherms, to Mr. J. van Wolput for IR measurements, to Ms. A. Elemans-Mehring for ICP-OES analyses, and to Mr. B. Mezari for NMR measurements.

References

[1] P.M.M. Blauwhoff, J.W. Gosselink, E.P. Kieffer, S.T. Sie, W.H.J. Stork, in: J. Weitkamp, L. Puppe (Eds.), Catalysis and Zeolites Fundamentals and Applications, Springer, New York, 1999.
[2] J.A. Moulijn, P.W.N.M. van Leeuwen, R.A. van Santen, Catalysis: An Integrated Approach to Homogeneous, Heterogeneous and Industrial Catalysis, Elsevier, Amsterdam, 1993.
[3] J.A. Biscardi, E. Iglesia, J. Catal. 182 (1999) 117.
[4] T. Waku, S.Y. Yu, E. Iglesia, Ind. Eng. Chem. Res. 42 (2003) 3680.
[5] Y. Li, J.N. Armor, Chem. Commun. (1997) 2013.
[6] R. Bulánek, K. Novoveská, B. Wichterlová, Appl. Catal. A 235 (2002) 181.
[7] H.-Y. Chen, W.M.H. Sachtler, Catal. Lett. 50 (1998) 125.
[8] H.-Y. Chen, T. Voskoboinikov, W.M.H. Sachtler, Catal. Today 54 (1999) 483.
[9] H.-Y. Chen, X. Wang, W.M.H. Sachtler, Phys. Chem. Chem. Phys. 2 (2000) 3083.
[10] F. Heinrich, C. Schmidt, E. Löffler, M. Menzel, W. Grünert, J. Catal. 212 (2002) 157.
[11] Q. Zhu, R.M. van Teeffelen, R.A. van Santen, E.J.M. Hensen, J. Catal. 221 (2004) 575.
[12] R.Q. Long, R.T. Yang, J. Catal. 207 (2002) 224.
[13] R.Q. Long, R.T. Yang, J. Am. Chem. Soc. 121 (1999) 5595.
[14] G.I. Panov, V.I. Sobolev, A.S. Kharitonov, J. Mol. Catal. 61 (1990) 85.
[15] G.I. Panov, CatTech 4 (2000) 18.
[16] P. Kubánek, B. Wichterlová, Z. Sobalík, J. Catal. 211 (2002) 109.
[17] E. Selli, A. Isernia, L. Forni, PCCP 2 (2002) 3301.
[18] E.J.M. Hensen, Q. Zhu, R.A. van Santen, J. Catal. 220 (2003) 260.
[19] J. Pérez-Ramírez, F. Kapteijn, K. Schöffel, J.A. Moulijn, Appl. Catal. B 44 (2003) 117.
[20] P. Ratnasamy, R. Kumar. Catal. Today 9 (1991) 329.
[21] V.L. Zholobenko, I.N. Senchenya, L.M. Kustov, V.B. Kazansky, Kinet. Catal. 32 (1991) 151.
[22] G.I. Panov, G.A. Sheveleva, A.S. Kharitonov, V.N. Romannikov, L.A. Vostrikova, Appl. Catal. A 82 (1992) 31.
[23] A.S. Kharitonov, G.A. Sheveleva, G.I. Panov, V.I. Sobolev, Y.A. Paukshtis, V.N. Romannikov, Appl. Catal. 98 (1993) 33.
[24] R. Burch, C. Howitt. Appl. Catal. A 103 (1993) 135.
[25] S. Bordiga, R. Buzzoni, F. Geobaldo, C. Lamberti, E. Giamello, A. Zecchina, G. Leofanti, G. Petrini, G. Tozzola, G. Vlaic, J. Catal. 158 (1996) 486.
[26] A.K. Uriarte, M.A. Rodkin, M.J. Gross, A.S. Kharithonov, G.I. Panov, Stud. Surf. Sci. Catal. 110 (1997) 857.
[27] J.L. Motz, H. Heinrichen, W.F. Hölderich, J. Mol. Catal. A 136 (1998) 175.
[28] A. Ribera, I.W.C.E. Arends, S. de Vries, J. Pérez-Ramírez, R.A. Sheldon, J. Catal. 195 (2000) 287.
[29] P. Notté, Top. Catal. 13 (2000) 387.
[30] P. Marturano, A. Kogelbauer, R. Prins, J. Catal. 190 (2000) 460.
[31] P. Marturano, L. Drozdová, A. Kogelbauer, R. Prins, J. Catal. 192 (2000) 236.
[32] K.A. Dubkov, N.S. Ovanesyan, A.A. Shteinman, E.V. Starokon, G.I. Panov, J. Catal. 207 (2002) 341.
[33] Q. Zhu, E.J.M. Hensen, B.L. Mojet, J.H.M.C. van Wolput, R.A. van Santen, Chem. Commun. (2002) 1232.
[34] Q. Zhu, B.L. Mojet, R.A.J. Janssen, E.J.M. Hensen, J. van Grondelle, P.C.M.M. Magusin, R.A. van Santen, Catal. Lett. 81 (2002) 205.
[35] G. Berlier, A. Zecchina, G. Spoto, G. Ricchiardi, S. Bordiga, C. Lamberti, J. Catal. 215 (2003) 264.
[36] G. Berlier, G. Spoto, S. Bordiga, G. Ricchiardi, P. Fisicaro, A. Zecchina, I. Rossetti, E. Selli, L. Forni, E. Giamello, C. Lamberti, J. Catal. 208 (2002) 64.
[37] D. Meloni, R. Monaci, V. Solinas, G. Berlier, S. Bordiga, I. Rossetti, C. Oliva, L. Forni, J. Catal. 214 (2003) 169.
[38] A.A. Battiston, J.H. Bitter, F.M.F. de Groot, A.R. Overweg, O. Stephan, J.A. van Bokhoven, P.J. Kooyman, C. van der Spek, G. Vankó, D.C. Koningsberger, J. Catal. 213 (2003) 251.
[39] P. Fejes, I. Kiricsi, K. Lázár, I. Marsi, A. Rockenbauer, L. Korecz, J.B. Nagy, R. Aiello, F. Testa, Appl. Catal. A 242 (2003) 247.
[40] E.J.M. Hensen, Q. Zhu, M.M.R.M. Hendrix, A.R. Overweg, P.J. Kooyman, M.V. Sychev, R.A. van Santen, J. Catal. 221 (2004) 560.
[41] E.J.M. Hensen, Q. Zhu, P.-H. Liu, K.-J. Chao, R.A. van Santen, J. Catal. 226 (2004) 466.
[42] G. Zi, T. Dake, Z. Ruiming, Zeolites 8 (1988) 453.
[43] T. Inui, H. Nagata, T. Takeguchi, S. Iwamoto, H. Matsuda, M. Inoue, J. Catal. 139 (1993) 482.
[44] D. Goldfarb, M. Bernardo, K.G. Strohmaier, D.E.W. Vaughan, H. Thomann, J. Am. Chem. Soc. 116 (1994) 6344.
[45] M. Santhosh Kumar, M. Schwidder, W. Grünert, A. Brückner, J. Catal. 227 (2004) 384.
[46] H. Lin, G. Coudurier, J.C. Vedrine, Stud. Surf. Sci. Catal. 49 (1989) 1431.
[47] Y. Han, X. Meng, H. Guan, Y. Yu, L. Zhao, X. Xu, X. Yang, S. Wu, N. Li, F. Xiao, Micropor. Mesopor. Mater. 57 (2003) 191.
[48] G. Berlier, G. Spoto, P. Fisicaro, S. Bordiga, A. Zecchina, E. Giamello, C. Lamberti, Microchem. J. 71 (2002) 101.
[49] J. Pérez-Ramírez, J. Catal. 227 (2004) 512.
[50] O.H. Han, C.-S. Kim, S.B. Hong, Angew. Chem. Int. Ed. 41 (2002) 469.
[51] A.V. McCormick, A.T. Bell, Catal. Rev. Sci. Eng. 31 (1989) 97.
[52] S. van Donk, A.H. Janssen, J.H. Bitter, K.P. de Jong, Catal. Rev. 45 (2003) 297.
[53] J. Pérez-Ramírez, F. Kapteijn, J.C. Groen, A. Doménech, G. Mul, J.A. Moulijn, J. Catal. 214 (2003) 33.
[54] A. Zecchina, S. Bordiga, G. Spoto, L. Marchese, G. Petrini, G. Leofanti, M. Padovan, J. Phys. Chem. 96 (1992) 4991.
[55] G. Mul, J. Pérez-Ramírez, F. Kapteijn, J.A. Moulijn, Catal. Lett. 80 (2002) 129.
[56] L.J. Lobree, I.-C. Hwang, J.A. Reimer, A.T. Bell, Catal. Lett. 63 (1999) 233.
[57] H.-Y. Chen, T. Voskovoinikov, W.M.H. Sachtler, J. Catal. 180 (1998) 171.
[58] G. Spoto, A. Zecchina, G. Berlier, S. Bordiga, M.G. Clerici, L. Basini, J. Mol. Catal. A 158 (2000) 107.
[59] M. Lezcano, V.I. Kovalchuk, J.L. d'Itri, Kinet. Catal. 42 (2001) 104.
[60] K. Segawa, Y. Chen, J.E. Kubsh, W.N. Delgass, J.A. Dumesic, W. Keith Hall, J. Catal. 76 (2001) 112.
[61] K. Hadjiivanov, J. Saussey, J.L. Freysz, J.C. Lavalley, Catal. Lett. 52 (1998) 103.
[62] G. Berlier, A. Zecchina, G. Spoto, G. Ricchiardi, S. Bordiga, C. Lamberti, J. Catal. 215 (2003) 264.
[63] E.F.T. Lee, L.V.C. Rees, Zeolites 7 (1987) 143.
[64] E.F.T. Lee, L.V.C. Rees, Zeolites 7 (1987) 219.
[65] J. Pérez-Ramírez, F. Kapteijn, G. Mul, J.A. Moulijn, Catal. Commun. 3 (2002) 19.

[66] J. Pérez-Ramírez, F. Kapteijn, A. Brückner, J. Catal. 218 (2002) 234.
[67] E.J.M. Hensen, Q. Zhu, R.A. van Santen, J. Catal. 233 (2005) 136.
[68] V.I. Sobolev, K.A. Dubkov, E.A. Paukshtis, L.V. Pirutko, M.A. Rodkin, A.S. Kharitonov, G.I. Panov, Appl. Catal. A 141 (1996) 185.
[69] G.D. Pirngruber, M. Luechinger, P.K. Roy, A. Cecchetto, P. Smirniotis, J. Catal. 224 (2004) 429.
[70] K.S. Pillai, J. Jia, W.M.H. Sachtler, Appl. Catal. 264 (2004) 133.
[71] K. Sun, H. Zhang, H. Xia, Y. Lian, Y. Li, Z. Feng, P. Ying, C. Li, Chem. Commun. (2004) 2480.